Received: 14 January 2022 | Revised: 3 June 2022 | Accepted: 10 August 2022

DOI: 10.1002/rnc.6345

RESEARCH ARTICLE

WILEY

Energy shaping control of underactuated mechanical systems with fluidic actuation

Enrico Franco[1] | **Alessandro Astolfi**[2,3]

[1]Mechanical Engineering Department, Imperial College London, London, UK

[2]Electrical and Electronic Engineering Department, Imperial College London, London, UK

[3]Dipartimento di Ingegneria Civile e Ingegneria Informatica, Università di Roma "Tor Vergata", Rome, Italy

Correspondence
Enrico Franco, Mechanical Engineering Department, Imperial College London, SW7 2AZ London, UK.
Email: e.franco11@imperial.ac.uk

Funding information
Engineering and Physical Sciences Research Council, Grant/Award Numbers: EP/R511547/1, EP/W004224/1, EP/W005557/1; Horizon 2020 Framework Programme, Grant/Award Number: 739551 (KIOS CoE); Italian Ministry for Research, Grant/Award Numbers: 2017YKXYXJ, 2020RTWES4

Abstract

Energy shaping is a remarkably effective control strategy which can be applied to a wide range of systems, including underactuated mechanical systems. However, research in this area has generally neglected actuator dynamics. While this is often appropriate, it might result in degraded performance in the case of fluidic actuation. In this work we present some new results on energy shaping control for underactuated mechanical systems for which the control action is mediated by a pressurized ideal fluid. In particular, we introduce an extended multi-step energy shaping and damping-assignment controller design procedure that builds upon the *Interconnection-and-damping-assignment Passivity-based-control* methodology in a modular fashion to account for the pressure dynamics of the fluid. Stability conditions are assessed with a Lyapunov approach, the effect of disturbances is discussed, and the case of redundant actuators is illustrated. The proposed approach is demonstrated with numerical simulations for a modified version of the classical ball-on-beam example, which employs two identical cylinders, either hydraulic or pneumatic, to actuate the beam.

KEYWORDS

energy shaping, fluidic actuation, nonlinear systems, underactuated mechanical systems

1 | INTRODUCTION

Energy shaping control has been successfully applied to a wide range of systems, including mechanical systems,[1,2] electro-mechanical and power systems,[3] nonholonomic systems described by kinematic models,[4] and recently soft continuum manipulators.[5] The *Interconnection-and-damping-assignment Passivity-based control* (IDA-PBC) methodology is particularly popular since it provides a physical interpretation of the control action within the port-Hamiltonian framework, and it does not rely on high gains.[6] Initial research on IDA-PBC focused on systems free from disturbances and from physical damping. The effect of damping was then investigated in References 7 and 8, while the effect of dissipative forces was accounted for in Reference 9. Recently, more sophisticated designs were proposed to compensate the effects of matched disturbances[10] and of unmatched disturbances under some structural assumptions.[11] In addition, the effect of input saturation was investigated in Reference 12.

Abbreviations: IDA-PBC, interconnection and damping assignment passivity-based control; PDEs, partial differential equations

Nevertheless, most of the research on IDA-PBC for mechanical systems has neglected actuator dynamics. A notable result in this respect is the study of weakly-coupled electro-mechanical systems presented in Reference 13. Although neglecting the actuator dynamics might be appropriate in some cases, provided for instance that the actuators have higher bandwidth compared to the mechanical system,[14] it might result in degraded performance in the case of fluidic actuation. With the term fluidic actuation we refer to all those cases where the control input acts on the system by means of a pressurized ideal fluid, either liquid or gas. Typical examples are hydraulic actuators, which are ubiquitous in tilt trailers, excavators, and cranes,[15,16] and pneumatic actuators, which are commonly employed in factory automation and in lightweight or compliant robots.[17,18] Fluidic actuation typically consists of a pressure source, supply pipes, a control valve, and a pump producing the control action in the form of a flow rate, and a cylinder transferring the forces to the mechanism. In some applications, including hydraulic tilt trailers and cranes, two or more cylinders can be arranged in antagonistic pairs to provide rotational motion while also resulting in redundant actuation.

From a theoretical viewpoint, fluidic actuation introduces a further challenge in the control of underactuated mechanical systems, since the control input is mediated by the pressure dynamics of the fluid. The study of systems characterized by fluid-structure interaction was first approached with a port-Hamiltonian model in Reference 19. Other notable results in this respect are the passivity-based control of a continuous-stirred tank reactor,[20] and the study of the stability conditions for boundary control in a 1-D spatial domain.[21] Port-Hamiltonian modeling and boundary energy shaping control of a compressible fluid in 1-D were presented in Reference 22. More recently, port-Hamiltonian modeling of two-phase flows was investigated in Reference 23. The passivity based control of a fully actuated double-acting hydraulic cylinder was outlined in Reference 24 by employing a locally linear dynamic assignment. Finally, the energy shaping control of a fully actuated hydraulic drive was presented in Reference 25, however the compressibility of the liquid was neglected. Besides energy shaping approaches, the study of fluid-structure interactions has also motivated research on systems characterized by cascades of partial-differential-equations (PDEs) by employing backstepping transformations and averaging in infinite dimensions.[26] Additionally, the open-loop control of a fluid in a pipe was investigated in Reference 27 by employing a flatness-based approach, while optimal control techniques were employed for the velocity-field control of an autonomous excavator fully actuated by hydraulic cylinders in Reference 16. In summary, the energy shaping control of underactuated mechanical systems with fluid-structure interactions has not been fully addressed to date. In our recent work,[28,29] we have investigated the energy shaping control of soft continuum manipulators with fluidic actuation. Nevertheless, the resulting controllers are only applicable to a narrow class of systems, and they do not include damping assignment, which is an integral part of IDA-PBC.

This work investigates the energy shaping control of underactuated mechanical system with fluidic actuation and presents the following new results.

- An extended multi-step energy shaping controller design procedure for underactuated mechanical systems with fluidic actuation is detailed. The proposed approach comprises potential energy shaping, kinetic energy shaping without imposing additional restrictions on the structure of the inertia matrix, and damping assignment, which was absent in References 28 and 29. In addition, it is applicable in the presence of redundant actuators. As a result, new matching conditions are obtained, while the PDEs that characterize the IDA-PBC for direct actuation are preserved.
- A new nonlinear control law, which applies to fluidic actuators characterized by a nonlinear relationship between volume and position is constructed, thus catering for different arrangements of hydraulic or pneumatic cylinders. Both isothermal liquids and ideal gases are considered.
- Stability conditions are assessed with a Lyapunov approach. The effect of vanishing bounded disturbances is discussed and compared to the baseline IDA-PBC.
- The proposed approach is demonstrated with numerical simulations for a modified ball-on-beam system which is actuated by two identical cylinders. Both hydraulic and pneumatic actuation are illustrated. The controller is compared with a traditional IDA-PBC design that neglects the pressure dynamics, and with an alternative algorithm constructed using a backstepping approach.

The rest of this article is organized as follows: the problem formulation is outlined in Section 2; the main result is detailed in Section 3; simulation results are presented in Section 4; concluding remarks are discussed in Section 5.

2 | PROBLEM FORMULATION

A brief overview of IDA-PBC[6] is provided for completeness. Subsequently, the system model considered in this work is defined.

2.1 | Overview of IDA-PBC

Consider an underactuated mechanical system with n degrees-of-freedom (DOFs) characterized by the Hamiltonian

$$H(q,p) = \frac{1}{2}p^T M(q)^{-1}p + \Omega(q), \tag{1}$$

where the inertia matrix is $M(q) = M(q)^T > 0$, and $\Omega(q)$ describes the potential energy. For ease of notation, M and $M(q)$ are used interchangeably throughout the article. The system states are the position $q \in \mathbb{R}^n$ and the momenta $p = M\dot{q} \in \mathbb{R}^n$. The system dynamics expressed in port-Hamiltonian form in the absence of disturbances is

$$\begin{bmatrix}\dot{q}\\ \dot{p}\end{bmatrix} = \begin{bmatrix}0 & I\\ -I & -D\end{bmatrix}\begin{bmatrix}\nabla_q H\\ \nabla_p H\end{bmatrix} + \begin{bmatrix}0\\ G\end{bmatrix}u, \quad y = G^T\nabla_p H. \tag{2}$$

The control input is $u(t) \in \mathbb{R}^m$ and the input matrix is $G(q) \in \mathbb{R}^{n\times m}$, with $\text{rank}(G) = m < n$ for all $q \in \mathbb{R}^n$ in case of underactuation. The term I indicates an identity matrix of appropriate dimension, $D = D^T \geq 0$ is the damping matrix, $\nabla_q H$ is the vector of partial derivatives of H with respect to q, and $\nabla_p H$ is the vector of partial derivatives with respect to p. The control aim of IDA-PBC corresponds to stabilizing the equilibrium $(q,p) = (q^*, 0)$, which can be unstable in open-loop but satisfies the admissibility condition $\nabla_q\Omega(q^*) = 0$ (i.e., it is an extremum of Ω), thus it is a regulation problem.

The IDA-PBC control law is constructed to achieve the closed-loop dynamics

$$\begin{bmatrix}\dot{q}\\ \dot{p}\end{bmatrix} = \begin{bmatrix}0 & M^{-1}M_d\\ -M_dM^{-1} & J_2 - D_d\end{bmatrix}\begin{bmatrix}\nabla_q H_d\\ \nabla_p H_d\end{bmatrix}, \tag{3}$$

where $H_d = \frac{1}{2}p^T M_d^{-1}p + \Omega_d$, and the closed-loop damping is defined as $D_d = (Gk_vG^T + DM^{-1}M_d)$. The design parameters in (3) are the potential energy Ω_d, the inertia matrix $M_d = M_d^T > 0$, the matrix $J_2 = -J_2^T$, and the constant gain matrix $k_v = k_v^T > 0$. The potential energy Ω_d should be defined such that it admits a strict minimizer $q^* = \text{argmin}(\Omega_d)$, thus the conditions $\nabla_q\Omega_d(q^*) = 0$ and $\nabla_q^2\Omega_d(q^*) > 0$ should be verified. Introducing the pseudo-inverse $G^\dagger = \left(G^TG\right)^{-1}G^T$, the IDA-PBC control law that achieves the closed-loop dynamics (3) is expressed as the sum of an energy shaping component u_{es}, which assigns the closed-loop equilibrium q^*, and a damping-assignment component u_{di}, which injects damping in the system through the parameter k_v, that is

$$\begin{aligned} u &= u_{\text{es}} + u_{\text{di}},\\ u_{\text{es}} &= G^\dagger\left(\nabla_q H - M_dM^{-1}\nabla_q H_d + J_2\nabla_p H_d\right),\\ u_{\text{di}} &= -k_vG^T\nabla_p H_d. \end{aligned} \tag{4}$$

To ensure matching between (2) and (3) on the unactuated states, M_d, J_2, and Ω_d should satisfy the set of PDEs

$$G^\perp\left(\nabla_q(p^TM^{-1}p) - M_dM^{-1}\nabla_q(p^TM_d^{-1}p) + 2J_2M_d^{-1}p\right) = 0, \tag{5}$$

$$G^\perp\left(\nabla_q\Omega - M_dM^{-1}\nabla_q\Omega_d\right) = 0, \tag{6}$$

where $G^\perp$ is a full-rank left annihilator of G, that is $G^\perp G = 0$ and $\text{rank}\left(G^\perp\right) = n - m$. If (5) and (6) are solvable for all $(q,p) \in \mathbb{R}^{2n}$, the control law (4) can be expressed analytically. Computing the time derivative of H_d and

substituting (3) yields

$$\dot{H}_d = -\nabla_p H_d^T D_d \nabla_p H_d \leq 0. \tag{7}$$

It follows that the equilibrium $(q,p) = (q^*,0)$ is asymptotically stable when $D = 0$ provided that the output $y = G^T \nabla_p H_d$ is detectable, since $D_d = G k_v G^T$ is rank deficient.[6] In addition, asymptotic stability can be concluded if the system has strong dissipation, that is $D_d > 0$ (see Lemma 4.2 in Reference 7). This latter condition can be met for some mechanical systems by setting $M_d = k_T M$ and $k_T > 0$ provided that $D > 0$ (see Reference 5 for details). It must be noted that (7) does not contain a negative-definite term in the position q. Consequently, the IDA-PBC control (4) is not inherently robust to disturbances, which has motivated research on more sophisticated designs such as Reference 10.

2.2 | System model

This work considers a mechanical system with $1 \leq m < n$ actuated DOFs indicated as $q_a = G^T q$ for conciseness, with the control input acting on the system by means of a pressurized ideal fluid, and satisfying the following assumptions.

Assumption 1. The fluid is isentropic and inviscid, and its bulk modulus Γ_0 is known. In addition, the pressure P of the fluid, its density ρ and speed v are bounded and uniform throughout its volume λ. Finally, the inertia M_0 of fluid, valves, pumps, and cylinders is negligible compared to the inertia M of the mechanism, that is $M \gg M_0$.

Assumption 2. The volume λ of fluid, which includes the supply pipes, only depends on the actuated position q_a. In addition, λ is a known and continuously differentiable function bounded away from zero, that is $\lambda > 0$.

Assumption 3. The PDEs (5) and (6) for the original system (1) with direct actuation are solvable analytically, and $q^* = \text{argmin}\,(\Omega_d)$. The closed-loop damping is either $D_d > 0$, or $D_d = G k_v G^T \geq 0$ in which case $y = G^T \nabla_p H_d$ is detectable. In addition, all trajectories of the closed-loop system (3) are bounded, and $(q,p) = (q^*,0)$ is an asymptotically stable equilibrium. Finally, all model parameters are exactly known, and all system states are measurable.

Assuming uniform pressure, uniform density, and uniform speed of the fluid is a reasonable approximation in case of laminar flow, while neglecting the effect of viscosity is appropriate at low speeds. The assumption made on the volume λ is satisfied by a wide range of cylinder arrangements (e.g., see Section 4). Neglecting the inertia of the fluid and the mass of the moving parts in valves, cylinders, and pumps is a reasonable approximation for hydraulic actuators in tilt trailers, excavators, and cranes. The analytical solvability of the PDEs is a research topic in itself,[3,30] thus it is not investigated further. Nevertheless, the PDEs (5) and (6) are solvable analytically for several canonical examples including the acrobot,[1] the disk-on-disk,[10] the inertia-wheel-pendulum,[31] and the ball-on-beam[6] which is illustrated in Section 4. Finally, the boundedness of the states in closed-loop (3) and the stability of the equilibrium for direct actuation follow from Reference 6.

The bulk modulus of a fluid is defined as

$$\Gamma_0 = -\lambda \frac{dP}{d\lambda} = -\rho \frac{dP}{d\rho}. \tag{8}$$

For isothermal liquids it is realistic to assume that the bulk modulus is constant.[32] Instead, computing (8) for an ideal gas with polytropic index c yields $\Gamma_0 = cP$. The mechanical energy of an isentropic fluid, if its inertia is neglected, corresponds to the internal energy

$$\Phi = -\int_{\lambda_0}^{\lambda} P d\lambda. \tag{9}$$

Considering at first an isothermal liquid and solving (8) yields $\rho = \rho_0 e^{P/\Gamma_0}$. Defining the specific internal energy $\phi = \frac{\Phi}{\rho\lambda}$ yields

$$\phi = \int_{\rho_0}^{\rho} \frac{P}{\rho^2} d\rho = \int_0^P \frac{P}{\Gamma_0} e^{-P/\Gamma_0} dP, \tag{10}$$

where $\rho_0 = 1$, for simplicity. Finally, computing $\Phi = \phi\rho\lambda$ from (10) yields[33]

$$\Phi = \left(-P + \Gamma_0(e^{P/\Gamma_0} - 1)\right)\lambda. \tag{11}$$

The pressure dynamics can be expressed as in Reference 34

$$\dot{P} = \Gamma_0 \frac{u - \dot{q}_a \nabla_q \lambda}{\lambda}, \tag{12}$$

where the volumetric flow rate u corresponds to the control input (i.e., $u > 0$ for inflow, while $u < 0$ for outflow). In practice, the flow rate can be provided by a control valve and a pump in response to a corresponding input voltage. Since the dynamics of pumps and valves is typically much faster than the pressure dynamics, these effects are neglected.

The complete system dynamics can be expressed as

$$\begin{bmatrix} \dot{q} \\ \dot{p} \\ \dot{P} \end{bmatrix} = \begin{bmatrix} 0 & I & 0 \\ -I & -D & \frac{\Gamma_0 \nabla_q \lambda}{\lambda} \\ 0 & -\frac{\Gamma_0 \nabla_q \lambda^T}{\lambda} & 0 \end{bmatrix} \begin{bmatrix} \nabla_q W \\ \nabla_p W \\ \nabla_P W \end{bmatrix} + \begin{bmatrix} 0 \\ 0 \\ 1 \end{bmatrix} \frac{\Gamma_0}{\lambda} u, \tag{13}$$

where $W = H + \Phi = \frac{1}{2} p^T M^{-1} p + \Omega + \Phi$, and the system states are now the position $q \in \mathbb{R}^n$, the momenta $p \in \mathbb{R}^n$, and the pressure $P \in \mathbb{R}^m$. In case $m > 1$, the energy of the fluid is computed as $\Phi = \sum_{i=1}^{m} \Phi_i$. Note that the input matrix G does not appear explicitly in (13). Instead, the control input affects the pressure dynamics, and the pressure contributes to the energy of the fluid (11) only with respect to the actuated positions since $\lambda(q_a)$ from Assumption 2, thus $\operatorname{rank}\left(\nabla_q \lambda\right) = m$. Computing $\dot{W}$ while substituting (13) yields $\dot{W} = -\nabla_p W^T D \nabla_p W + \nabla_P W^T \frac{\Gamma_0}{\lambda} u$. Thus system (13) is passive with respect to u and $y' = \frac{\Gamma_0}{\lambda} \nabla_P W$, and the product $u^T y'$ has unit of power. Since the aim of this work is to account for the pressure dynamics of an ideal fluid by building upon the traditional IDA-PBC in a modular fashion, the output $y = G^T \nabla_p H_d$ of (3) remains of interest.

Considering an ideal gas with polytropic index c and computing Φ from (9) yields

$$\Phi = \begin{cases} P\lambda \log\left(\frac{\lambda_0}{\lambda}\right) & c = 1 \\ -\frac{P\lambda^c}{c-1}\left(\lambda_0^{1-c} - \lambda^{1-c}\right) & c \neq 1, \end{cases} \tag{14}$$

where $\lambda_0 > 0$ is the initial value of λ. Computing the total energy W from (14), the complete system dynamics is still given by (13), where $\Gamma_0 = cP$. Thus (13) represents the starting point for the controller design with either isothermal liquids or ideal gases.

3 | MAIN RESULT

This section presents an extended energy shaping and damping assignment procedure that builds upon the IDA-PBC (4) to account for the pressure dynamics of an ideal fluid. To streamline the presentation, Section 3.1 outlines the controller design for systems without disturbances or redundant actuators, which is the reference condition for IDA-PBC.[6] Subsequently, the effect of disturbances is discussed in Section 3.2, while the case of redundant actuation is discussed in Section 3.3.

3.1 | Energy shaping and damping assignment

The control law for system (13) is designed such that the closed-loop dynamics in port-Hamiltonian form becomes

$$\begin{bmatrix} \dot{q} \\ \dot{p} \\ \dot{P} \end{bmatrix} = \begin{bmatrix} 0 & S_{12} & S_{13} \\ -S_{12}^T & -S_{22} & S_{23} \\ -S_{13}^T & -S_{23}^T & -S_{33} \end{bmatrix} \begin{bmatrix} \nabla_q W_d \\ \nabla_p W_d \\ \nabla_P W_d \end{bmatrix}, \tag{15}$$

where $W_d = H_d + \frac{1}{2}\zeta^T\zeta = \frac{1}{2}p^T M_d^{-1} p + \Omega_d + \frac{1}{2}\zeta^T\zeta$ is a positive definite storage function, and $\zeta \in \mathbb{R}^m$ is defined as

$$\zeta = G^{\dagger}\left(-\nabla_q H - \nabla_q \Phi + M_d M^{-1}\nabla_q H_d + \frac{\Gamma_0 \nabla_q \lambda}{\lambda}\nabla_P \Phi + \left(G k_v G^T - J_2\right) M_d^{-1} p\right). \tag{16}$$

The terms S_{ij}, with $1 \leq i,j \leq 3$, are computed according to the following procedure in order for the open-loop dynamics (13) to match the closed-loop dynamics (15) on all DOFs.

Step 1: This step aims to preserve the relationship between the position q and the momenta p. Equating the first rows of (13) and of (15) yields

$$M^{-1}p = S_{12}\nabla_p H_d + S_{12}\zeta\frac{\partial \zeta}{\partial p} + S_{13}\zeta\frac{\partial \zeta}{\partial P}. \tag{17}$$

Setting $S_{12} = M^{-1}M_d$ and $S_{13} = -S_{12}\frac{\partial \zeta}{\partial p}\left(\frac{\partial \zeta}{\partial P}\right)^{-1}$ verifies (17). Note that the matrix $\frac{\partial \zeta}{\partial P} \in \mathbb{R}^{m\times m}$ is a function of λ, thus it follows from Assumption 2 that it is invertible.

Step 2: This step corresponds to the IDA-PBC energy shaping procedure in Section 2.1, which is modified here to account for the pressurized fluid and for the damping assignment. Equating the second rows of (13) and of (15) yields

$$-\nabla_q H - \nabla_q \Phi - D M^{-1} p + \frac{\Gamma_0 \nabla_q \lambda}{\lambda}\nabla_P \Phi = -S_{12}^T \nabla_q H_d - S_{12}^T \zeta\frac{\partial \zeta}{\partial q} - S_{22}\nabla_p H_d - S_{22}\zeta\frac{\partial \zeta}{\partial p} + S_{23}\zeta\frac{\partial \zeta}{\partial P}. \tag{18}$$

Substituting $S_{22} = DM^{-1}M_d + Gk_vG^T - J_2$, the physical damping D on the left side of (18) vanishes. Defining the pseudo-inverse $G^{\otimes} = (G^{\perp}G^{\perp T})^{-1}G^{\perp}$ and pre-multiplying both sides of (18) by either $G^{\otimes}$ or by $G^{\dagger}$ while refactoring terms gives the two new matching conditions

$$G^{\otimes}\left(-\nabla_q H + S_{12}^T \nabla_q H_d - J_2 \nabla_p H_d\right) = G^{\otimes}\left(-S_{12}^T \zeta\frac{\partial \zeta}{\partial q} - S_{22}\zeta\frac{\partial \zeta}{\partial p} + S_{23}\zeta\frac{\partial \zeta}{\partial P}\right), \tag{19}$$

$$G^{\dagger}\left(-\nabla_q H - \nabla_q \Phi + \frac{\Gamma_0 \nabla_q \lambda}{\lambda}\nabla_P \Phi + S_{12}^T \nabla_q H_d + \left(G k_v G^T - J_2\right)\nabla_p H_d\right) = G^{\dagger}\left(-S_{12}^T \zeta\frac{\partial \zeta}{\partial q} - S_{22}\zeta\frac{\partial \zeta}{\partial p} + S_{23}\zeta\frac{\partial \zeta}{\partial P}\right). \tag{20}$$

Equation (19) enforces matching on the unactuated DOFs, and its left-hand side corresponds to the sum of the PDEs (5) and (6). Instead, Equation (20) enforces matching on the actuated DOFs. The term S_{23} is thus defined as

$$S_{23} = G\left(1 + G^{\dagger}S_{12}^T\frac{\partial \zeta}{\partial q} + G^{\dagger}S_{22}\frac{\partial \zeta}{\partial p}\right)\left(\frac{\partial \zeta}{\partial P}\right)^{-1} + G^{\perp T}\left(G^{\otimes}S_{12}^T\frac{\partial \zeta}{\partial q} + G^{\otimes}S_{22}\frac{\partial \zeta}{\partial p}\right)\left(\frac{\partial \zeta}{\partial P}\right)^{-1}. \tag{21}$$

Substituting (21) into (19) yields $G^{\perp}\left(-\nabla_q H + M_d M^{-1}\nabla_q H_d - J_2\nabla_p H_d\right) = 0$, thus preserving the PDEs (5) and (6) as well as their analytical solutions M_d, J_2, and Ω_d (see Assumption 3). In addition, (21) verifies (20) thus ensuring matching for the actuated DOFs. In summary, the proposed design procedure yields the new matching conditions (19) and (20) but results in the same PDEs as the traditional IDA-PBC (4), thus it is applicable to the same class of system that was given in Reference 6 in terms of solvability of the aforementioned PDEs.

Step 3: Equating the third rows of (13) and of (15) yields

$$\Gamma_0\frac{u - \dot{q}_a\nabla_q\lambda}{\lambda} = -S_{13}^T\nabla_q W_d - S_{23}^T\nabla_p W_d - S_{33}\zeta\frac{\partial \zeta}{\partial P}, \tag{22}$$

where S_{33} is defined as

$$S_{33} = K_i\left(\frac{\partial \zeta}{\partial P}^T\frac{\partial \zeta}{\partial P}\right)^{-1}, \tag{23}$$

with $K_i > 0$ a constant parameter matrix. Computing the control input u from (22) yields

$$u = \dot{q}_a\nabla_q\lambda - \frac{\lambda}{\Gamma_0}\left(S_{13}^T\nabla_q W_d + S_{23}^T\nabla_p W_d + S_{33}\zeta\frac{\partial \zeta}{\partial P}\right), \tag{24}$$

where $S_{12}, S_{13}, S_{22}, S_{23}, S_{33}$ have been defined previously. Energy shaping of the mechanical system is achieved through the terms M_d, J_2, and Ω_d in ζ, while damping assignment is achieved through k_v in S_{22} and in ζ. Finally, shaping of the internal energy of the fluid (11) or (14) is achieved through the parameter K_i.

Proposition 1. *Consider the system (13) with Assumptions 1 to 3, in closed-loop with the control law (24). Then the equilibrium $(q, p, P) = (q^*, 0, P^*)$ is asymptotically stable for all $K_i > 0$ provided that either $D_d > 0$ or that $D_d = Gk_vG^T \geq 0$ and the output $y = G^T\nabla_p H_d$ of the original system (3) is detectable.*

Proof. Computing the time derivative of W_d and substituting (15) while recalling that $J_2 = -J_2^T$ yields

$$\begin{aligned}\dot{W}_d &= -\nabla_p W_d^T D_d \nabla_p W_d - \zeta^T K_i \zeta \\ &= -x^T D_d x - \zeta^T K_i \zeta \leq 0,\end{aligned} \tag{25}$$

where $x = (M_d^{-1}p + \zeta\frac{\partial\zeta}{\partial p})$.

Case 1: If $D_d > 0$ it follows from (25) that $\zeta, p \in \mathcal{L}^2 \cap \mathcal{L}^\infty$. Computing $\dot{p}$ from (15) yields $\dot{p} \in \mathcal{L}^\infty$, thus p is bounded and converges to zero asymptotically.[35] It follows from (15) that $\dot{P} \in \mathcal{L}^\infty$, thus computing $\dot{\zeta}$ from (16) yields $\dot{\zeta} \in \mathcal{L}^\infty$ and consequently ζ converges to zero asymptotically. Substituting $\dot{p} = p = 0$ and $\zeta = 0$ in (15) yields $\nabla_q\Omega_d = 0$, thus the equilibrium is an extremum of Ω_d. In addition, $q^* = \text{argmin}(\Omega_d)$ by hypothesis. Substituting $p = 0$ and $\zeta = 0$ in (16) yields

$$G^\dagger\left(-\nabla_q\Omega - \nabla_q\Phi + M_d M^{-1}\nabla_q\Omega_d + \frac{\Gamma_0\nabla_q\lambda}{\lambda}\nabla_P\Phi\right) = 0, \tag{26}$$

which, computed at $q = q^*$, defines the pressure at the equilibrium P^*. Thus, the equilibrium $(q, p, P) = (q^*, 0, P^*)$ is asymptotically stable.

Case 2: If $D_d = Gk_vG^T \geq 0$ then it follows from (25) that $\dot{W}_d \leq -\chi_{\min}(k_v)|G^Tx|^2 - \chi_{\min}(K_i)|\zeta|^2 \leq 0$, where $\chi_{\min}(\cdot)$ indicates the minimum eigenvalue of a matrix, and $G^Tx = y + G^T\zeta\frac{\partial\zeta}{\partial p}$. Thus $p \in \mathcal{L}^\infty$ and $\zeta, y \in \mathcal{L}^2 \cap \mathcal{L}^\infty$, while computing the time derivative of p from (15) and of ζ from (16) yields $\dot{p}, \dot{\zeta} \in \mathcal{L}^\infty$ hence y and ζ converge to zero. Asymptotic stability of the equilibrium can be established in a similar fashion to Reference 6 provided that y is detectable (see Theorem 3.2 in Reference 36). ∎

Remark 1. The controller design procedure is applicable to systems with non-constant inertia matrix and non-trivial kinetic shaping. In particular, the design is considerably simplified if $k_v = 0, J_2 = 0$, and $M_d = k_T M$ as in Reference 29, since ζ would not depend on the momenta p thus resulting in $S_{13} = 0$. While it is possible to account for the inertia M_0 of fluid, valves, pumps, and cylinders within (13), that would result in a different inertia matrix $M' = M + M_0$. Therefore, the analytical solution of the kinetic-energy PDE (5) would have to be computed on a case-by-case basis, depending on the specific arrangement of the actuators. However, since M_0 only depends on the actuated DOFs, the kinetic-energy PDE would remain solvable analytically for certain classes of systems, including those with underactuation degree $n - m = 1$ and with M' that only depends on q_a.[30] Future work shall focus on the analytical solution of the kinetic-energy PDE accounting for the inertia of the fluid. A further direction that could be explored corresponds to employing an algebraic solutions of the PDEs similarly to Reference 3.

3.2 | External forces

This section investigates the effect of the external forces δ affine in the momenta p within (13), that is

$$\begin{bmatrix}\dot{q}\\ \dot{p}\\ \dot{P}\end{bmatrix} = \begin{bmatrix}0 & I & 0\\ -I & -D & \frac{\Gamma_0\nabla_q\lambda}{\lambda}\\ 0 & -\frac{\Gamma_0\nabla_q\lambda^T}{\lambda} & 0\end{bmatrix}\begin{bmatrix}\nabla_q W\\ \nabla_p W\\ \nabla_P W\end{bmatrix} - \begin{bmatrix}0\\ \delta\\ 0\end{bmatrix} + \begin{bmatrix}0\\ 0\\ 1\end{bmatrix}\frac{\Gamma_0}{\lambda}u,$$

which are accounted for in *Step 2* of the energy shaping procedure by introducing an additional vector Λ of closed-loop non-conservative forces, as defined in Reference 11. Thus, the potential-energy PDE (6) can be rewritten as

$$G^{\perp}\left(\nabla_q \Omega - M_d M^{-1} \nabla_q \left(\Omega_d - \Omega_0\right)\right) = 0, \tag{27}$$

$$G^{\perp}\left(\delta - M_d M^{-1} \nabla_q \Omega_0\right) = 0, \tag{28}$$

where $\Omega_0 = \Lambda^T(q - q^*)$. Again, it is assumed here that both (27) and (28) are solvable analytically for the original system with direct actuation. Since external forces might not be accurately known, for instance due to sensor noise, a further assumption is introduced.

Assumption 4. The external forces $\delta \in \mathbb{R}^n$ are bounded, that is $|\delta| \leq \epsilon$ for some known $\epsilon > 0$, and $|\delta - \epsilon| \leq |\epsilon_0(t)|$, with $\epsilon_0(t) \in \mathcal{L}^2 \cap \mathcal{L}^\infty$ representing a bounded vanishing disturbance. In addition, the equilibrium q^* is assignable, that is $G^{\perp}(\nabla_q \Omega(q^*) + \delta) = 0$ and the PDEs (27) and (28) are solvable analytically.

The design procedure in Section 3.1 is modified by redefining the term ζ in (16) as

$$\zeta = G^{\dagger}\left(-\nabla_q H - \nabla_q \Phi + M_d M^{-1} \nabla_q H_d - \epsilon + M_d M^{-1} \Lambda + \frac{\Gamma_0 \nabla_q \lambda}{\lambda} \nabla_P \Phi + \left(G k_v G^T - J_2\right) M_d^{-1} p\right). \tag{29}$$

The structure of the control law (24) does not change, however it now contains the constant bound ϵ and the vector Λ within ζ. In addition, the measurement error $\epsilon_0(t)$ is accounted for in the closed-loop dynamics (15) as

$$\begin{bmatrix} \dot{q} \\ \dot{p} \\ \dot{P} \end{bmatrix} = \begin{bmatrix} 0 & S_{12} & S_{13} \\ -S_{12}^T & -S_{22} & S_{23} \\ -S_{13}^T & -S_{23}^T & -S_{33} \end{bmatrix} \begin{bmatrix} \nabla_q W_d \\ \nabla_p W_d \\ \nabla_P W_d \end{bmatrix} - \begin{bmatrix} 0 \\ \epsilon_0(t) \\ 0 \end{bmatrix}.$$

Proposition 2. *Consider the system (13) with Assumptions 1 to 4, in closed-loop with the control law (24), where ζ is defined in (29). Then the following claims hold.*

- *The system trajectories are bounded if $(D_d - I/4) > 0$ and $K_i|\zeta|^2 > |\epsilon_0(t)|^2$.*
- *The equilibrium is asymptotically stable if $|\epsilon_0(t)| \leq \gamma |\nabla_p W_d|$ for some $\gamma > 0$ provided that $(D_d - \gamma I) > 0$ and $K_i > 0$.*

Proof. Computing the time derivative of W_d and substituting (15) while accounting for the external forces δ yields

$$\begin{aligned} \dot{W}_d &= -\nabla_p W_d^T D_d \nabla_p W_d + \nabla_p W_d^T (\epsilon - \delta) - \zeta^T K_i \zeta \\ &\leq -\nabla_p W_d^T \left(D_d - \frac{I}{4}\right) \nabla_p W_d - K_i |\zeta|^2 + |\epsilon_0(t)|^2, \end{aligned} \tag{30}$$

where the second line has been obtained by using Young's inequality $\nabla_p W_d^T |\epsilon_0(t)| \leq \frac{1}{4} \nabla_p W_d^T \nabla_p W_d + |\epsilon_0(t)|^2$.

It follows from (30) that $\dot{W}_d \leq 0$ if $(D_d - I/4) > 0$ and $K_i|\zeta|^2 > |\epsilon_0(t)|^2$, with $\epsilon_0(t) \in \mathcal{L}^2 \cap \mathcal{L}^\infty$ by hypothesis, thus the trajectories of the closed-loop system are bounded.[37] To prove the second claim substitute $|\epsilon_0(t)| \leq \gamma |\nabla_p W_d|$ in the first line of (30), which yields $\dot{W}_d \leq 0$ provided that $(D_d - \gamma I) > 0$ and $K_i > 0$. Asymptotic stability is concluded employing the same arguments as Proposition 1. A similar claim holds if the disturbances are matched (i.e., $\delta = G\delta_0$) provided that $k_v > \gamma$ and $K_i > 0$, and that $y = G^T \nabla_p H_d$ is detectable. ∎

Remark 2. If the disturbance $\epsilon_0(t)$ is non-vanishing, boundedness of the trajectories of the closed-loop system can be concluded from Lemma 5.3 in Reference 37. Local asymptotic stability of the equilibrium can be concluded for some classes of unknown external forces by introducing in the control law either an integral action[10] or adaptive observers[11] to compensate the effect of δ. This approach has been illustrated for a specific class of systems in References 5 and 38, thus it is not discussed further. For comparison purposes, accounting for the external forces δ within the baseline IDA-PBC design in Section 2.1 and computing the time derivative of H_d as in (7) yields

$$\begin{aligned} \dot{H}_d &= -p^T M_d^{-1} D_d M_d^{-1} p + p^T M_d^{-1} (\epsilon - \delta) \\ &\leq -p^T M_d^{-1} \left(D_d - \frac{I}{4}\right) M_d^{-1} p + |\epsilon_0(t)|^2. \end{aligned} \tag{31}$$

It is apparent that (31) lacks the quadratic term in ζ which appears instead in (30). Intuitively, this indicates that explicitly accounting for the pressure dynamics of the fluid has beneficial effects on stability compared to treating this phenomenon as yet another disturbance or to disregarding it altogether.

3.3 | Redundant fluidic actuation

In engineering practice, multiple pressures P_j can be associated to the same actuated DOF. This is the case when two single-acting cylinders with volumes λ_1 and λ_2 are employed in an antagonistic pair to achieve bidirectional motion (see Section 4). Thus, the total energy is $W = H + \Phi_1(\lambda_1, P_1) + \Phi_2(\lambda_2, P_2)$ and the closed-loop dynamics (15) becomes

$$\begin{bmatrix} \dot{q} \\ \dot{p} \\ \dot{P}_1 \\ \dot{P}_2 \end{bmatrix} = \begin{bmatrix} 0 & S_{12} & S_{13} & S_{14} \\ -S_{12}^T & -S_{22} & S_{23} & S_{24} \\ -S_{13}^T & -S_{23}^T & -S_{33} & S_{34} \\ -S_{14}^T & -S_{24}^T & -S_{34}^T & -S_{44} \end{bmatrix} \begin{bmatrix} \nabla_q W_d \\ \nabla_p W_d \\ \nabla_{P_1} W_d \\ \nabla_{P_2} W_d \end{bmatrix}, \tag{32}$$

where $W_d = H_d + \frac{1}{2}\zeta^T\zeta$, and ζ is defined as

$$\zeta = G^\dagger \left(-\nabla_q H - \nabla_q \Phi_1 - \nabla_q \Phi_2 + M_d M^{-1} \nabla_q H_d + \frac{\Gamma_0 \nabla_q \lambda_1}{\lambda_1} \nabla_{P_1} \Phi_1 + \frac{\Gamma_0 \nabla_q \lambda_2}{\lambda_2} \nabla_{P_2} \Phi_2 + \left(G k_v G^T - J_2 \right) M_d^{-1} p \right). \tag{33}$$

The terms S_{12}, S_{22} are defined as in Section 3.1, while $S_{34} = 0$ considering that the pressures in the different actuators do not interact directly. The matching conditions corresponding to (19) and (20) now include the additional terms S_{14}, S_{24} which refer to the redundant actuator of volume λ_2. Thus $S_{13}, S_{14}, S_{23}, S_{24}$ are defined as

$$\begin{aligned} S_{13} &= -\frac{1}{2} S_{12} \frac{\partial \zeta}{\partial p} \left(\frac{\partial \zeta}{\partial P_1} \right)^{-1}, \quad S_{14} = -\frac{1}{2} S_{12} \frac{\partial \zeta}{\partial p} \left(\frac{\partial \zeta}{\partial P_2} \right)^{-1}, \\ S_{23} &= \frac{1}{2} G \left(1 + G^\dagger S_{12}^T \frac{\partial \zeta}{\partial q} + G^\dagger S_{22} \frac{\partial \zeta}{\partial p} \right) \left(\frac{\partial \zeta}{\partial P_1} \right)^{-1} + \frac{1}{2} G^{\perp T} \left(G^\otimes S_{12}^T \frac{\partial \zeta}{\partial q} + G^\otimes S_{22} \frac{\partial \zeta}{\partial p} \right) \left(\frac{\partial \zeta}{\partial P_1} \right)^{-1}, \\ S_{24} &= \frac{1}{2} G \left(1 + G^\dagger S_{12}^T \frac{\partial \zeta}{\partial q} + G^\dagger S_{22} \frac{\partial \zeta}{\partial p} \right) \left(\frac{\partial \zeta}{\partial P_2} \right)^{-1} + \frac{1}{2} G^{\perp T} \left(G^\otimes S_{12}^T \frac{\partial \zeta}{\partial q} + G^\otimes S_{22} \frac{\partial \zeta}{\partial p} \right) \left(\frac{\partial \zeta}{\partial P_2} \right)^{-1}. \end{aligned} \tag{34}$$

Note that S_{13} and S_{14} have a similar structure, differing only due to their dependence on P_1 or P_2. The same property applies to S_{23} and S_{24}.

The pressure dynamics for each hydraulic actuator is given by

$$\begin{aligned} \Gamma_0 \frac{u_1 - \dot{q}_a \nabla_q \lambda_1}{\lambda_1} &= -S_{13}^T \nabla_q W_d - S_{23}^T \nabla_p W_d - S_{33} \zeta \frac{\partial \zeta}{\partial P_1}, \\ \Gamma_0 \frac{u_2 - \dot{q}_a \nabla_q \lambda_2}{\lambda_2} &= -S_{14}^T \nabla_q W_d - S_{24}^T \nabla_p W_d - S_{44} \zeta \frac{\partial \zeta}{\partial P_2}, \end{aligned} \tag{35}$$

where $S_{33} = K_i \left(\frac{\partial \zeta}{\partial P_1}^T \frac{\partial \zeta}{\partial P_1} \right)^{-1}$ and $S_{44} = K_i \left(\frac{\partial \zeta}{\partial P_2}^T \frac{\partial \zeta}{\partial P_2} \right)^{-1}$. Computing the control input from (35) yields

$$\begin{aligned} u_1 &= \dot{q}_a \nabla_q \lambda_1 - \frac{\lambda_1}{\Gamma_0} \left(S_{13}^T \nabla_q W_d + S_{23}^T \nabla_p W_d + S_{33} \zeta \frac{\partial \zeta}{\partial P_1} \right), \\ u_2 &= \dot{q}_a \nabla_q \lambda_2 - \frac{\lambda_2}{\Gamma_0} \left(S_{14}^T \nabla_q W_d + S_{24}^T \nabla_p W_d + S_{44} \zeta \frac{\partial \zeta}{\partial P_2} \right). \end{aligned} \tag{36}$$

Asymptotic stability of the equilibrium can be concluded following the same reasoning of Proposition 1. The general case of multiple redundant actuators, although less common in practice, can be treated in a similar fashion and is omitted for brevity.

Remark 3. In case of pneumatic actuation, the control input can be expressed in terms of the mass flow rate u', rather than the volumetric flow rate u. Thus, substituting $u_1 = u_1' \frac{R_s T}{P_1}$ and $u_2 = u_2' \frac{R_s T}{P_2}$ in (13), where $\rho_1 = \frac{P_1}{R_s T}$ and $\rho_2 = \frac{P_2}{R_s T}$ are the densities of the ideal gas in either cylinder, and solving (35) with $\Gamma_{0_1} = cP_1$ and $\Gamma_{0_2} = cP_2$ respectively yields the control laws

$$u_1' = \frac{\dot{q}_a \nabla_q \lambda_1 P_1}{R_s T} - \frac{\lambda_1}{c R_s T}\left(S_{13}^T \nabla_q W_d + S_{23}^T \nabla_p W_d + S_{33}\zeta \frac{\partial \zeta}{\partial P_1}\right),$$
$$u_2' = \frac{\dot{q}_a \nabla_q \lambda_2 P_2}{R_s T} - \frac{\lambda_2}{c R_s T}\left(S_{14}^T \nabla_q W_d + S_{24}^T \nabla_p W_d + S_{44}\zeta \frac{\partial \zeta}{\partial P_2}\right), \tag{37}$$

where T is the temperature in Kelvin, R_s is the specific gas constant, and c is the polytropic index. Note that, differently from (36), the control laws (37) also depend on the temperature.

4 | SIMULATION RESULTS

The ball-on-beam system is revisited here by introducing two identical single-acting cylinders that push against the beam with a sliding contact (see Figure 1). The cylinders form an antagonistic pair and, in case of hydraulic actuation, they are supplied by two volumetric pumps with flow rates u_1 and u_2. The volumes λ_1, λ_2 of fluid in the cylinders are nonlinear functions of the inclination of the beam q_2, that is

$$\lambda_1 = A\left(L_0 + \frac{L}{2}\tan(q_2)\right), \quad \lambda_2 = A\left(L_0 - \frac{L}{2}\tan(q_2)\right). \tag{38}$$

The pressure of the fluid in the cylinders is denoted by P_1 and P_2, respectively. The equations of motion of the ball-on-beam with direct actuation, under some assumptions on the masses for simplicity, are given by (2) with the parameters

$$M = \begin{bmatrix} 1 & 0 \\ 0 & L^2 + q_1^2 \end{bmatrix}, \quad G = \begin{bmatrix} 0 \\ 1 \end{bmatrix}, \quad \Omega = g q_1 \sin(q_2), \tag{39}$$

where q_1 is the position of the ball, q_2 is the inclination of the beam, L is half the length of the beam, and g is the gravity constant.[6] In practice, $|q_1| \leq L$ and $|q_2| < \pi/2$ with the proposed constructive solution. The prescribed equilibrium is $(q_1^*, q_2^*) = (0, 0)$. The IDA-PCB design (4) for direct actuation yields

$$M_d = \left(L^2 + q_1^2\right)\begin{bmatrix} \sqrt{\frac{2}{(L^2+q_1^2)}} & 1 \\ 1 & \sqrt{2\left(L^2 + q_1^2\right)} \end{bmatrix}, J_2 = \left(p_1 - p_2\sqrt{\frac{2}{\left(L^2 + q_1^2\right)}}\right)\begin{bmatrix} 0 & 1 \\ -1 & 0 \end{bmatrix},$$
$$\Omega_d = g - g\cos(q_2) + \frac{k_p}{2}\left(q_2 - \frac{1}{\sqrt{2}}\operatorname{arcsinh}\left(\frac{q_1}{L}\right)\right)^2, \tag{40}$$

where k_p is a positive tuning parameter and the damping assignment is governed by the parameter k_v.[6] Since the two cylinders result in redundant actuation, the control law is computed using (36) for isothermal liquids, and using (37) for ideal gases. According to Assumption 1, the inertia M_0 of fluid, valves, cylinders, and pumps is neglected. Additionally,

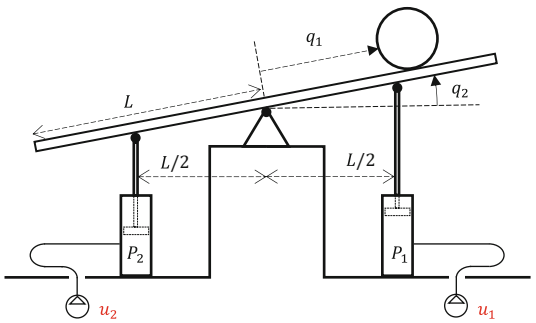

FIGURE 1 Simplified schematic of the ball-on-beam system with fluidic actuation. Each single-acting cylinder is supplied by a control valve and a pump providing the flow rates u_1 and u_2. The cylinders push against the beam with a sliding contact.

no physical damping is present, that is $D = 0$. The control laws (36) and (37) employ the parameters (40), which are the solutions of the PDEs (5) and (6) for the ball-on-beam system with direct actuation.[6] The IDA-PBC for direct actuation (4) and a backstepping algorithm (see Appendix A) are employed for comparison purposes.

4.1 | Hydraulic actuation

Simulations have been conducted in MATLAB with an ODE23 solver using the model parameters in SI units $L = 0.5, g = 9.81, A = 10^{-5}, L_0 = 1, \Gamma_0 = 2 \times 10^9$ (i.e., corresponding to water, assumed isothermal), with the initial conditions $(q_1, q_2, \dot{q}_1, \dot{q}_2, P_1, P_2) = (0.45, 0, 0, 0, 2 \times 10^6, 2 \times 10^6)$. The time history of the states and of the control input computed with (36), where $\frac{\partial \zeta}{\partial P_1} = -\frac{\partial \zeta}{\partial P_2} = AL\left(1 + \tan(q_2)^2\right)/2$, using the tuning parameters $k_p = 1, k_v = 1, K_i = 1$ is shown in Figure 2 for different values of L_0. The position converges to $(q_1^*, q_2^*) = (0, 0)$ in a smooth fashion, and the pressures P_1 and P_2, in [bar], converge to their initial values at equilibrium. The control input increases with L_0, while the time history of the position

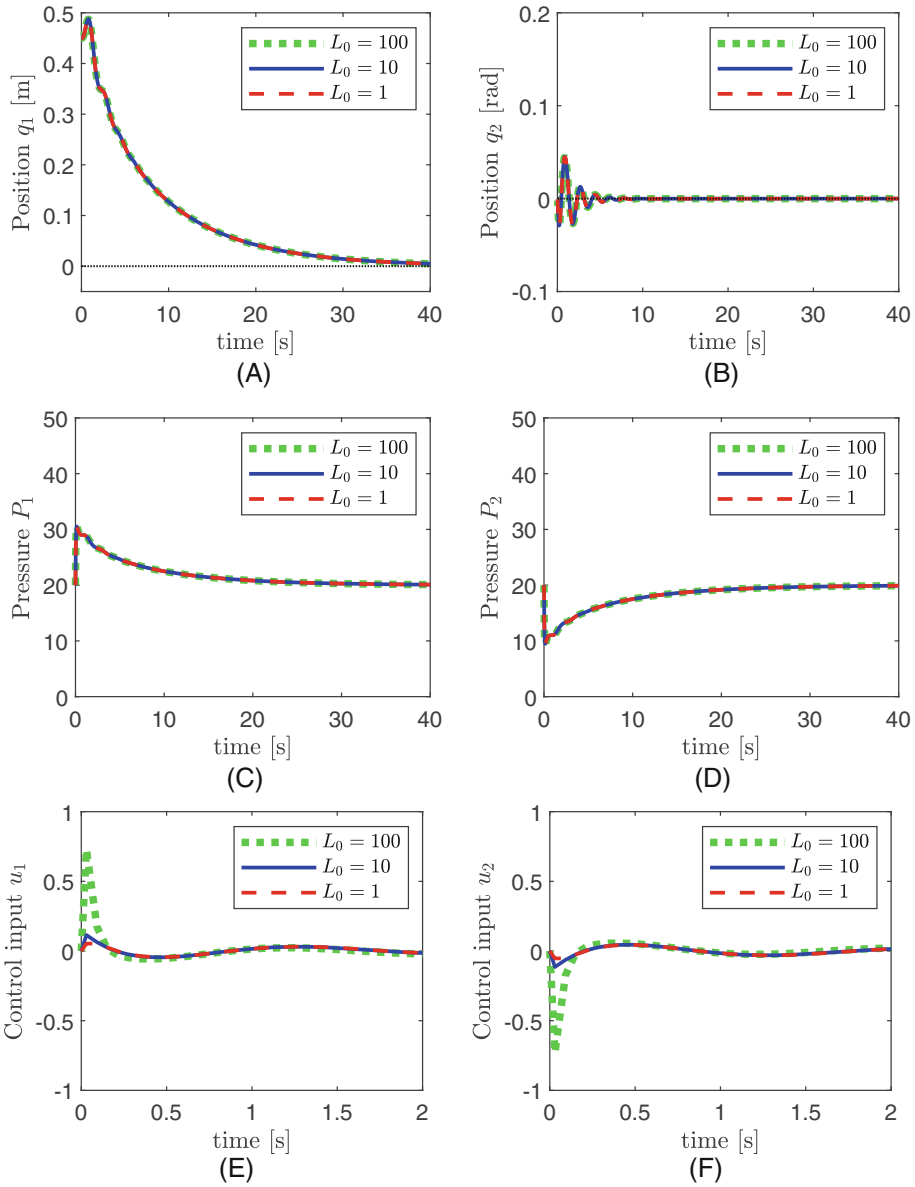

FIGURE 2 Simulation results with hydraulic actuation and controller (36) for different values of L_0: (A) Position q_1; (B) position q_2; (C) pressure P_1; (D) pressure P_2; (E) control input u_1 during the initial transient; (F) control input u_2

shows no noticeable difference. This indicates that reducing the dead volume of fluid (e.g., by mounting the control valves near the cylinders) can reduce the control effort, in accordance with engineering practice.

For comparison purposes, the system response with the traditional IDA-PBC controller (4) and the parameters (40) is shown in Figure 3. In this case the tuning parameters were chosen empirically as $k_p = 50, k_v = 100$ to obtain a similar transient to that in Figure 2, while u_1, u_2 were computed as

$$u_1 = \frac{2u}{ALK_0}, \; u_2 = -\frac{2u}{ALK_0}, \tag{41}$$

where $K_0 = 2 \times 10^7$ is an additional tuning parameter that accounts for the bulk modulus of the fluid, and u is given in (4). The simulations indicate that neglecting the pressure dynamics in the controller results in an oscillatory response and in larger pressure variations, which are particularly noticeable for a larger L_0 and might lead to loss of contact between the cylinders and the beam (e.g., in case $P_1 = 0$ or $P_2 = 0$). Note also that the pressures P_1 and P_2 at the equilibrium vary with L_0 and are larger than with the controller (36) in some cases (e.g., for $L_0 = 1$), which indicates a higher energy consumption. While a smoother transient can be achieved in this case by reducing k_p or increasing k_v, this also results in

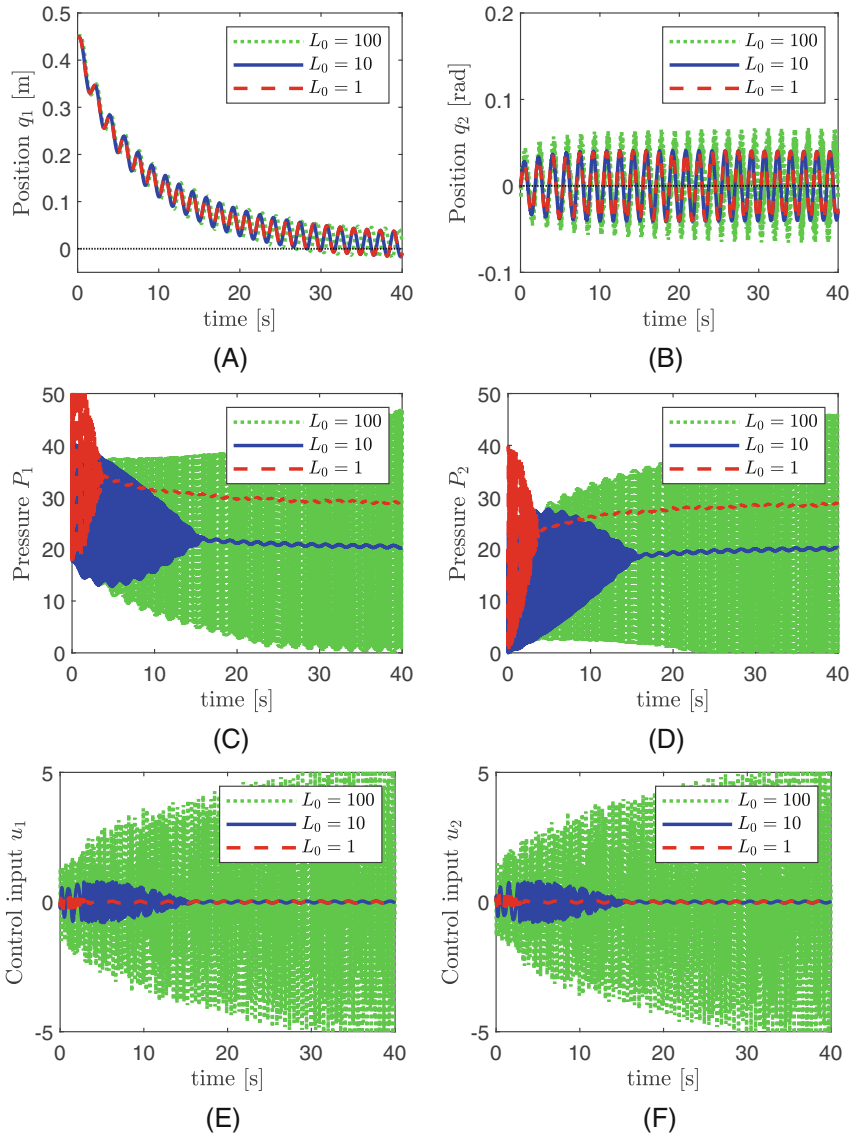

FIGURE 3 Simulation results with hydraulic actuation and controller (41) for different values of L_0: (A) Position q_1; (B) position q_2; (C) pressure P_1; (D) pressure P_2; (E) control input u_1; (F) control input u_2

a slower response. In addition, simultaneously increasing k_p, k_v, and K_0 slightly reduces the amplitude of the oscillations on the position. However, using high gains could amplify the effect of sensor noise on the measured states in practice. Conversely, simultaneously decreasing k_p, k_v, and K_0 results in larger oscillations on the position and in higher peak pressures.

In summary, the new controller (36) yields a smoother response and a reduced magnitude of the control input compared to the baseline IDA-PBC (41), which does not take into account the pressure dynamics of the fluid. This could be beneficial in engineering practice, since a smaller control action could allow employing smaller and less expensive control valves, and smoother movements could reduce vibrations in the mechanism. Nevertheless, the improved performance comes at the cost of having to provide pressure measurements with suitable sensors.

4.2 | Pneumatic actuation

The simulation results for pneumatic actuation are shown in Figure 4. In this case, the control law is computed using (37), where $R_s = 287$, $T = 293$, and the polytropic index is $c = 1.5$, corresponding to adiabatic expansion for an ideal gas.

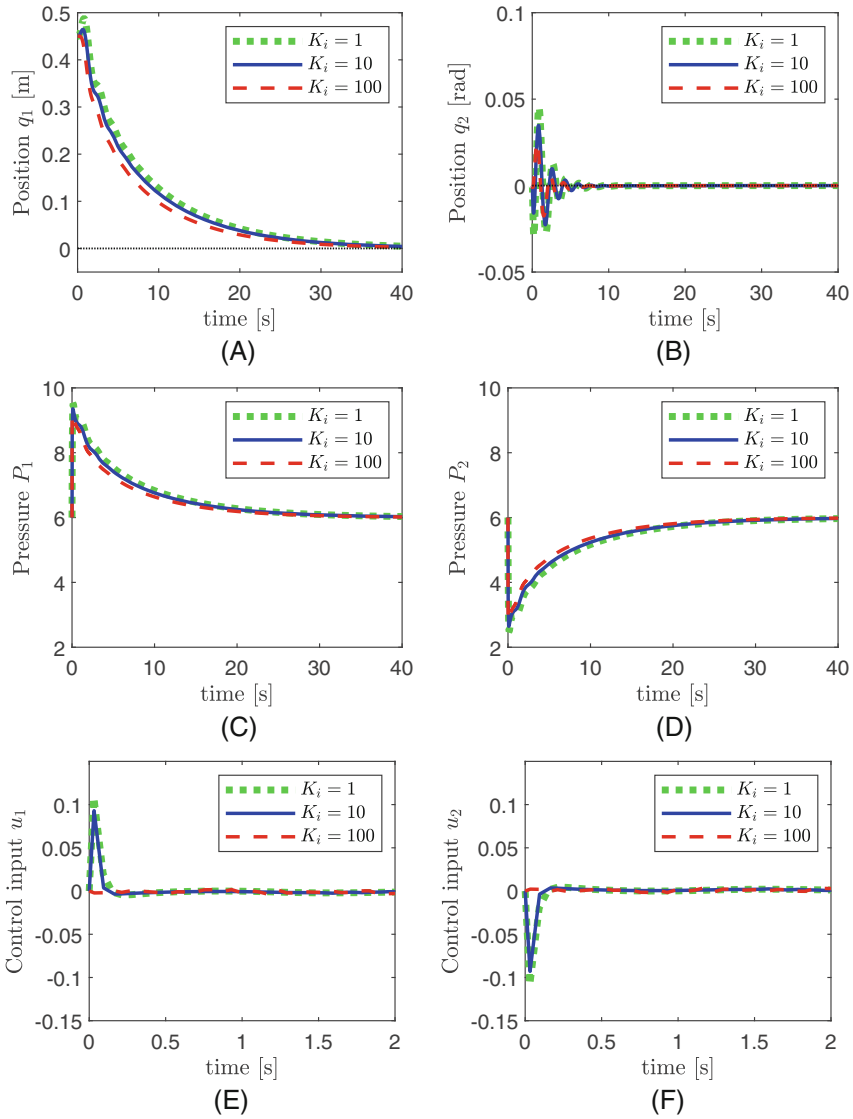

FIGURE 4 Simulation results with pneumatic actuation and controller (37) for different values of K_i: (A) Position q_1; (B) position q_2; (C) pressure P_1; (D) pressure P_2; (E) control input u_1' during the initial transient; (F) control input u_2'

In this case the internal energy of the gas is given by (14), thus $\frac{\partial \zeta}{\partial P_1} = -\frac{\partial \zeta}{\partial P_2} = AL/\left(2\cos(q_2)^2\right)$. The area of the cylinders is set to $A = 3 \times 10^{-5}$ so that the pressures vary within a range representative of industrial air supply (i.e., $P_1, P_2 \leq 10$ bar). The remaining model parameters and the tuning parameters are the same as for the hydraulic actuation (i.e., $L_0 = 100$ in this case), and the initial conditions are $(q_1, q_2, \dot{q}_1, \dot{q}_2, P_1, P_2) = (0.45, 0, 0, 0, 6 \times 10^5, 6 \times 10^5)$. The system response is similar to that in Figure 2, and the pressures P_1 and P_2 converge to their initial values at equilibrium, in [bar]. However, the control input is considerably smaller, since in this case it corresponds to the mass flow rate of gas into the cylinders. The effect of the model parameter L_0 is similar to the case of hydraulic actuation, thus it is not shown. Increasing the value of the tuning parameter K_i yields a slightly faster response and slightly smaller peak pressures, and it also considerably reduces the control effort during the initial transient (see Figure 4E,F). This can be explained by noting that K_i introduces a dissipative effect on the pressure dynamics in (15). Finally, the transient response depends also on the tuning parameters k_p and k_v in (40) according to the IDA-PBC design (4). Employing the IDA-PBC controller (4) with (40) while computing u_1' and u_2' in a similar fashion to (41) yields similar results to those in Figure 3, which are omitted for brevity. Compared to the ball-on-beam system with direct actuation and with the IDA-PBC (4) (see Appendix B), the proposed controller yields a similar transient response with the same values of k_p and k_v. The initial overshoot and the slightly longer settling time

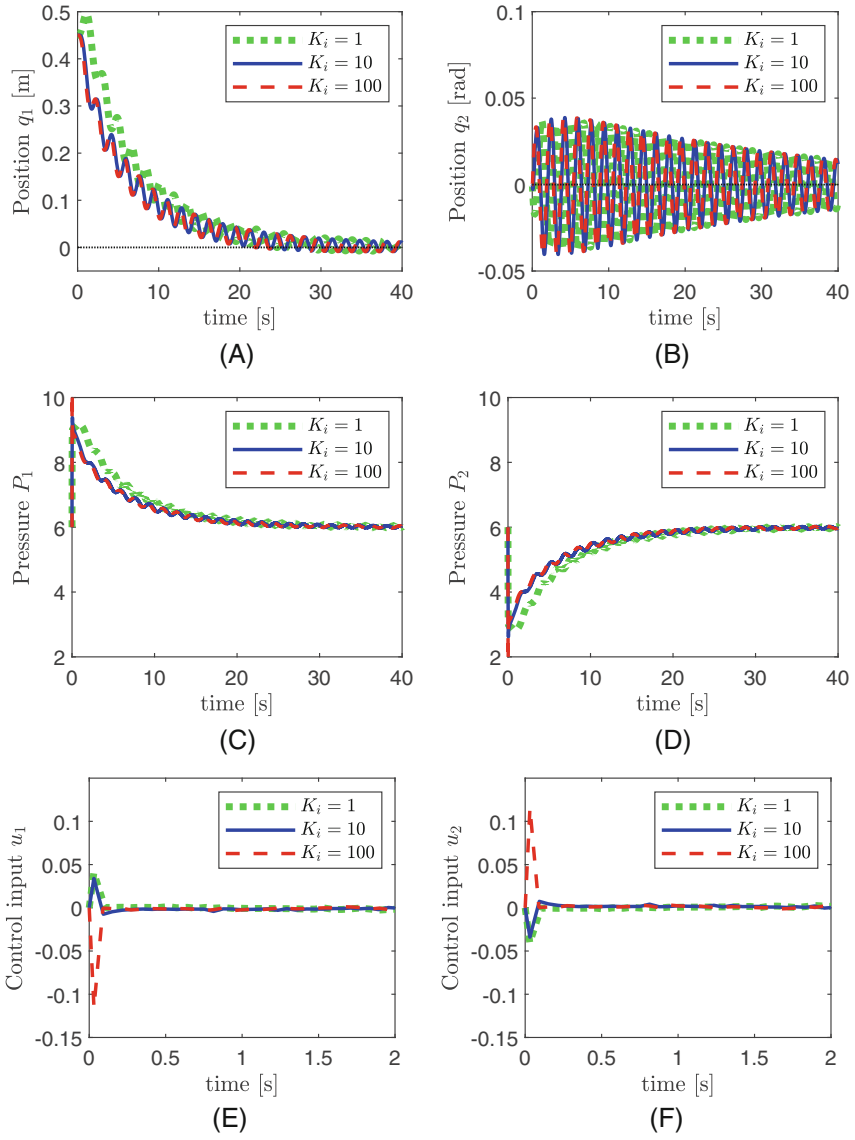

FIGURE 5 Simulation results with pneumatic actuation and backstepping algorithm (A1) for different values of K_i: (A) Position q_1; (B) position q_2; (C) pressure P_1; (D) pressure P_2; (E) control input u_1' during the initial transient; (F) control input u_2'

observed in Figure 4A for $K_i = 1$ are due to the pressure dynamics and can be reduced by increasing K_i (e.g., see $K_i = 100$ in Figure 4A).

For comparison purposes, a backstepping algorithm has been constructed based on the IDA-PBC (4) to account for the pressure dynamics of the ideal gas (see Appendix A). Figure 5 shows that the backstepping algorithm (A1) with the tuning parameters $k_p = 1, k_v = 10, K_i = 1$, chosen empirically to achieve a similar response to that of controller (37), is superior to the baseline IDA-PBC (41). However, the system response is more oscillatory than with the controller (37), which is agreement with our prior work.[28] Increasing the value of K_i in the backstepping algorithm also slightly improves the responsiveness, but differently from Figure 4, it does not reduce the control effort. Finally, the effect of a bounded vanishing disturbance acting on the ball, that is $\delta = \epsilon_0[\cos(q_2)\tanh(\dot{q}_1) \;\; 0]$ with $\epsilon_0 = -0.1$, is shown in Figure 6. The new controller (37) yields a similar response to that in Figure 4 with the same tuning parameters (i.e., in this case $K_i = 100$ and $\epsilon = 0$ in (29)). Instead, the backstepping algorithm (A1) and the baseline IDA-PBC result in oscillations of increasing amplitude, with the baseline IDA-PBC eventually leading to instability hence confirming the analysis in Remark 2.

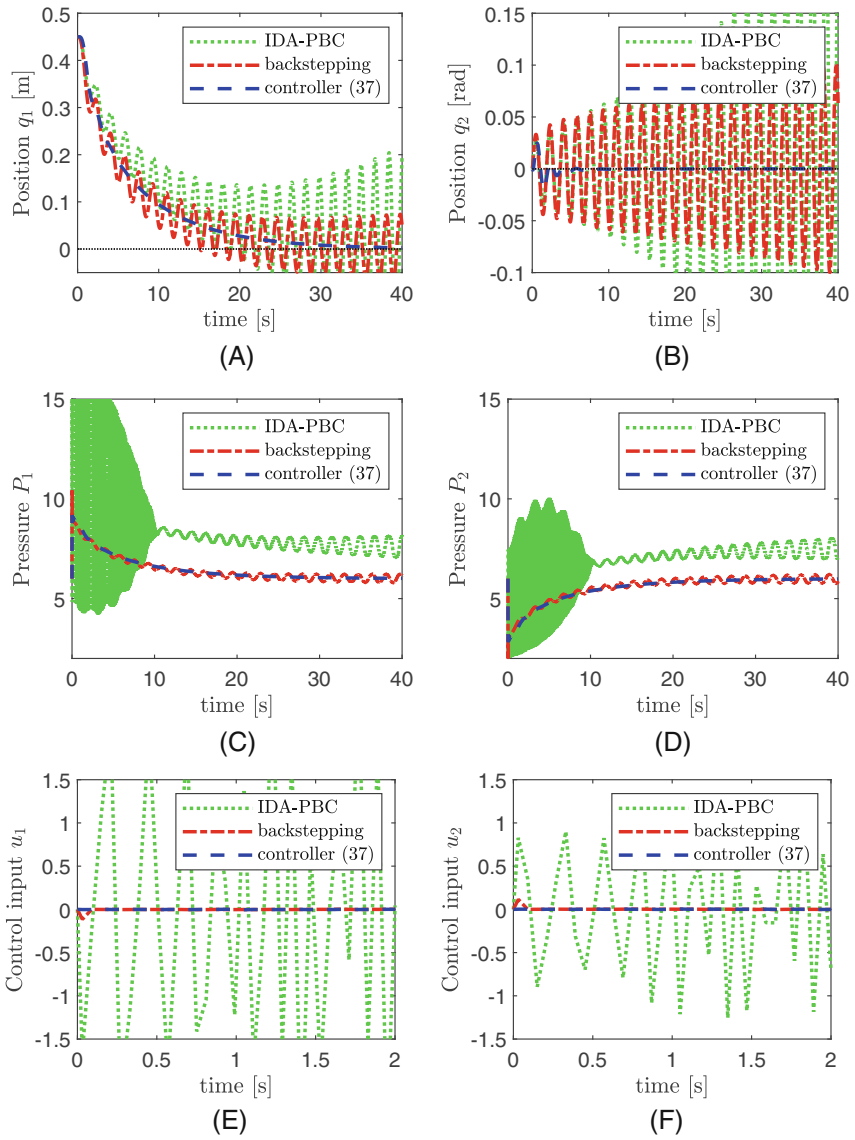

FIGURE 6 Simulation results with pneumatic actuation and bounded vanishing disturbances comparing the traditional IDA-PBC (4), the backstepping algorithm (A1), and the new controller (37): (A) Position q_1; (B) position q_2; (C) pressure P_1; (D) pressure P_2; (E) control input u_1' during the initial transient; (F) control input u_2'

5 | CONCLUSION

This article presented some new results on the energy shaping control for underactuated mechanical systems for which the control action is mediated by a pressurized ideal fluid. Building upon the IDA-PBC methodology in a modular fashion, an extended multi-step energy shaping and damping-assignment controller design procedure was outlined for both isothermal liquids and ideal gases. In addition, the effect of bounded vanishing disturbances and the case of redundant actuators were discussed.

Simulation results for a ball-on-beam system actuated by two identical cylinders, either hydraulic or pneumatic, indicate that the controller is effective in achieving the prescribed regulation goal, while yielding a smoother transient and a reduced control effort compared to the baseline IDA-PBC. The performance improvement is particularly noticeable in the presence of larger dead volumes of fluid. Further reductions of the control effort, together with moderate improvements in responsiveness, can be achieved by appropriately tuning the additional parameter introduced in the controller design procedure. The proposed controllers also yield a smoother response compared to an alternative backstepping algorithm based on IDA-PBC for direct actuation. The difference in performance is particularly noticeable in the presence of bounded vanishing disturbances.

Future work will aim to extend these results by accounting for the inertia of the fluid in the energy shaping procedure, and eventually for the internal dynamics of different types of actuators, including valves and pumps.

FUNDING INFORMATION

Engineering and Physical Sciences Research Council (Grant agreement No EP/W004224/1, EP/R511547/1, and EP/W005557/1). European Union's Horizon 2020 Research and Innovation Programme under Grant agreement No 739551 (KIOS CoE). Italian Ministry for Research (2017 Program for Research Projects of National Interest under Grant 2017YKXYXJ, and 2020 Program for Research Projects of National Interest under Grant 2020RTWES4).

CONFLICT OF INTEREST

The authors declared that they have no conflict of interest to this work.

DATA AVAILABILITY STATEMENT

The data that support the findings of this study are available from the corresponding author upon reasonable request.

ORCID

Enrico Franco https://orcid.org/0000-0001-9991-7377
Alessandro Astolfi https://orcid.org/0000-0002-4331-454X

REFERENCES

1. Mahindrakar AD, Astolfi A, Ortega R, Viola G. Further constructive results on interconnection and damping assignment control of mechanical systems: the Acrobot example. *Int J Robust Nonlinear Control*. 2006;16(14):671-685.
2. Hao S, Yamashita Y, Kobayashi K. Robust passivity-based control design for active nonlinear suspension system. *Int J Robust Nonlinear Control*. 2022;32(1):373-392. doi:10.1002/rnc.5827
3. Nunna K, Sassano M, Astolfi A. Constructive interconnection and damping assignment for port-controlled Hamiltonian systems. *IEEE Trans Automat Contr*. 2015;60(9):2350-2361.
4. Yi B, Ortega R, Zhang W. Smooth, time-invariant regulation of non-holonomic systems via energy pumping-and-damping. *Int J Robust Nonlinear Control*. 2020;30(16):6399-6413. doi:10.1002/rnc.5109
5. Franco E, Garriga-Casanovas A, Tang J, y Baena FR, Astolfi A. Adaptive energy shaping control of a class of nonlinear soft continuum manipulators. *IEEE ASME Trans Mechatron*. 2022;27(1):280-291.
6. Ortega R, Spong MW, Gomez-Estern F, Blankenstein G. Stabilization of a class of underactuated mechanical systems via interconnection and damping assignment. *IEEE Trans Automat Contr*. 2002;47(8):1218-1233.
7. Gómez-Estern F, Van der Schaft AJ. Physical damping in IDA-PBC controlled underactuated mechanical systems. *Eur J Control*. 2004;10(5):451-468.
8. Sandoval J, Kelly R, Santibáñez V. Interconnection and damping assignment passivity-based control of a class of underactuated mechanical systems with dynamic friction. *Int J Robust Nonlinear Control*. 2011;21(7):738-751.
9. Donaire A, Ortega R, Romero JG. Simultaneous interconnection and damping assignment passivity-based control of mechanical systems using dissipative forces. *Syst Control Lett*. 2016;8(94):118-126.
10. Donaire A, Romero JG, Ortega R, Siciliano B. Robust IDA-PBC for underactuated mechanical systems subject to matched disturbances. *Int J Robust Nonlinear Control*. 2017;27(6):1000-1016.

11. Franco E, Rodriguez Y, Baena F, Astolfi A. Robust dynamic state feedback for underactuated systems with linearly parameterized disturbances. *Int J Robust Nonlinear Control*. 2020;30(10):4112-4128.
12. Harandi J, Reza M, Taghirad HD, Molaei A, Romero JG. Bounded inputs total energy shaping for a class of underactuated mechanical systems. *Int J Robust Nonlinear Control*. 2021;31(18):9267-9281.
13. Ryalat M, Laila DS, ElMoaqet H, Almtireen N. Dynamic IDA-PBC control for weakly-coupled electromechanical systems. *Automatica*. 2020;5(115):108880.
14. Ortega R, Yi B, Romero JG. Robustification of nonlinear control systems vis-à-vis actuator dynamics: an immersion and invariance approach. *Syst Control Lett*. 2020;12(146):104811.
15. Kim J, Jin M, Choi W, Lee J. Discrete time delay control for hydraulic excavator motion control with terminal sliding mode control. *Mechatronics*. 2019;6(60):15-25.
16. Kim K, Kim M, Kim D, Lee D. Modeling and velocity-field control of autonomous excavator with main control valve. *Automatica*. 2019;6(104):67-81.
17. Della Santina C, Katzschmann RK, Bicchi A, Rus D. Model-based dynamic feedback control of a planar soft robot: trajectory tracking and interaction with the environment. *Int J Robot Res*. 2020;39(4):490-513.
18. Bu N, Liu H, Li W. Robust passive tracking control for an uncertain soft actuator using robust right coprime factorization. *Int J Robust Nonlinear Control*. 2021;31(14):6810-6825.
19. Cardoso-Ribeiro FL, Matignon D, Pommier-Budinger V. Modeling of a fluid-structure coupled system using port-Hamiltonian formulation. *IFAC-PapersOnLine*. 2015;10(28):217-222.
20. Ramírez H, Le Gorrec Y, Maschke B, Couenne F. On the passivity based control of irreversible processes: a port-Hamiltonian approach. *Automatica*. 2016;64:105-111.
21. Ramirez H, Zwart H, Le Gorrec Y. Stabilization of infinite dimensional port-Hamiltonian systems by nonlinear dynamic boundary control. *Automatica*. 2017;11(85):61-69.
22. Macchelli A, Le Gorrec Y, Ramírez H. Boundary energy-shaping control of an ideal compressible isentropic fluid in 1-D. *IFAC-PapersOnLine*. 2017;50(1):5598-5603.
23. Bansal H, Schulze P, Abbasi MH, et al. Port-Hamiltonian formulation of two-phase flow models. *Syst Control Lett*. 2021;3(149):104881.
24. Kotyczka P, Koch G, Pellegrini E, Lohmann B. Transparent parametrization of nonlinear IDA-PBC for a hydraulic actuator. *IFAC-PapersOnLine*. 2010;9(43):1122-1127.
25. Kogler H, Schöberl M, Scheidl R, Schö Berl M, Scheidl R. Passivity-based control of a pulse-width mode operated digital hydraulic drive. *J Syst Control Eng*. 2019;233(6):656-665.
26. Oliveira TR, Krstic M. Extremum seeking boundary control for PDE–PDE cascades. *Syst Control Lett*. 2021;9(155):105004.
27. Kopp J, Woittennek F. Flatness based trajectory planning and open-loop control of shallow-water waves in a tube. *Automatica*. 2020;12(122):109251.
28. Franco E, Ayatullah T, Sugiharto A, Garriga Casanovas A, Virdyawan V. Nonlinear energy-based control of soft continuum pneumatic manipulators. *Nonlinear Dyn*. 2021;106(1):229-253.
29. Franco E. Energy shaping control of hydraulic soft continuum planar manipulators. *IEEE Control Syst Lett*. 2022;6:1748-1753. https://ieeexplore.ieee.org/document/9638969/
30. Acosta JA, Ortega R, Astolfi A, Mahindrakar AD. Interconnection and damping assignment passivity-based control of mechanical systems with underactuation degree one. *IEEE Trans Automat Contr*. 2005;50(12):1936-1955.
31. Ryalat M, Laila DS. A simplified IDA-PBC design for underactuated mechanical systems with applications. *Eur J Control*. 2016;27:1-16.
32. Hayward ATJ. How to measure the isothermal compressibility of liquids accurately. *J Phys D Appl Phys*. 1971;4(7):938-950.
33. Gao L, Mei W, Kleeberger M, Peng H, Fottner J. Modeling and discretization of hydraulic actuated telescopic boom system in port-Hamiltonian formulation. Proceedings of the 9th International Conference on Simulation and Modeling Methodologies, Technologies and Applications, SCITEPRESS - Science and Technology Publications; 2019:69-79.
34. Acuna-Bravo W, Canuto E, Malan S, Colombo D, Forestello M, Morselli R. Fine and simplified dynamic modelling of complex hydraulic systems. Proceedings of the American Control Conference; 2009:5480-5485; IEEE.
35. Tao G. A simple alternative to the Barbalat lemma. *IEEE Trans Automat Contr*. 1997;42(5):698.
36. Byrnes CI, Isidori A, Willems JC. Passivity, feedback equivalence, and the global stabilization of minimum phase nonlinear systems. *IEEE Trans Automat Contr*. 1991;36(11):1228-1240.
37. Khalil H. *Nonlinear Systems*. 2nd ed. Prentice-Hall; 1996.
38. Franco E, Garriga Casanovas A, Donaire A. Energy shaping control with integral action for soft continuum manipulators. 2021;4(158):104250.
39. Krstic M, Kanellakopoulos I, Kokotovic P. *Nonlinear and Adaptive Control Design*. Adaptive and Learning Systems for Signal Processing, Communications and Control Series. Wiley; 1995.

How to cite this article: Franco E, Astolfi A. Energy shaping control of underactuated mechanical systems with fluidic actuation. *Int J Robust Nonlinear Control*. 2022;32(18):10011-10028. doi: 10.1002/rnc.6345

APPENDIX A

A backstepping procedure[39] is employed to design an alternative controller for the ball-on-beam system (39) with pneumatic actuation based on the IDA-PBC (4). To this end, we define the virtual control input $u^* = \frac{2u}{AL}$ representing the pressure differential between the two cylinders, where u is given in (4) with the design parameters (40). We introduce the terms $\varsigma_1 = P_1 - P_0 - u^*$ and $\varsigma_2 = P_2 - P_0 + u^*$, where P_0 is a constant representing the pressure at equilibrium. The control laws u_1' and u_2' are defined as

$$u_1' = -\frac{AL\dot{q}_2 P_1\left(1+\tan(q_2)^2\right)}{2R_sT} + \frac{A\left(\dot{u}^* - K_i\varsigma_1 + \frac{ALG^TM_d^{-1}p}{2\cos(q_2)^2}\right)\left(L_0 + \frac{L}{2}\tan(q_2)\right)}{R_sTc}$$
$$u_2' = \frac{AL\dot{q}_2 P_2\left(1+\tan(q_2)^2\right)}{2R_sT} + \frac{A\left(-\dot{u}^* - K_i\varsigma_2 + \frac{ALG^TM_d^{-1}p}{2\cos(q_2)^2}\right)\left(L_0 - \frac{L}{2}\tan(q_2)\right)}{R_sTc}, \tag{A1}$$

where K_i is a constant tuning parameter and $\dot{u}^*$ is the time derivative of u^* computed by substituting $\dot{q}$ and $\dot{p}$ from (2).

Defining the Lyapunov function candidate $\Psi = H_d + \frac{1}{2}\varsigma_1^2 + \frac{1}{2}\varsigma_2^2$ and computing its time derivative along the trajectories of (13) while substituting u_1' and u_2' from (A1) yields thus

$$\dot{\Psi} = -\nabla_p H_d^T D_d \nabla_p H_d - K_i\left(\varsigma_1^2 + \varsigma_2^2\right) \leq 0, \tag{A2}$$

which has a similar structure to (25). Nevertheless, in this case the closed-loop dynamics is not port-Hamiltonian.[28]

APPENDIX B

System response for the ball-on-beam system with direct actuation obtained with the traditional IDA-PBC design (4) and the parameters (40). The tuning parameters are $k_p = 1, k_v = 1$ and the initial conditions are $(q_1, q_2, \dot{q}_1, \dot{q}_2) = (0.45, 0, 0, 0)$ (Figure B1).

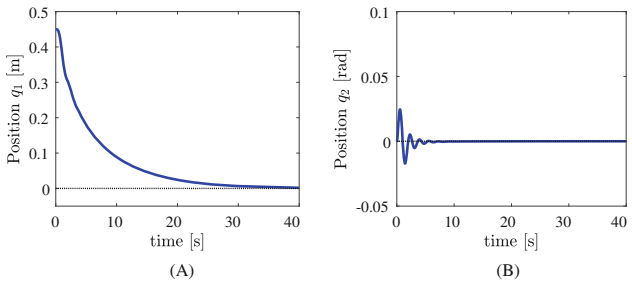

FIGURE B1 Simulation results for ball-on-beam system with direct actuation and IDA-PBC (4): (A) Position q_1; (B) position q_2